Detuning optimization of nonlinear mistuned bladed-disks

Evangéline Capiez-Lernout, Christian Soize

Turbo Expo 2022
June 13 - June 17, 2022, Rotterdam, The Netherlands

DETUNING OPTIMIZATION OF NONLINEAR MISTUNED BLADED-DISKS

Evangéline Capiez-Lernout*
Université Gustave Eiffel
MSME UMR 8208 CNRS
5, Bd Descartes
77454 Marne-la-Vallée
Email: evangeline.capiez-lernout@univ-eiffel.fr

Christian Soize
Université Gustave Eiffel
MSME UMR 8208 CNRS
5, Bd Descartes
77454 Marne-la-Vallée
Email: christian.soize@univ-eiffel.fr

ABSTRACT

One major industrial challenge is to consider the detuning as a technological means to reduce the dynamical amplifications induced by mistuning. Due to technological evolutions, the nonlinear geometrical effects induced by the large displacements cannot longer be neglected. Recently, methodologies for the robust analysis of detuned/mistuned bladed-disks in presence of geometrical nonlinearities have been developed. A full analysis of the detuning optimization of mistuned bladed-disks with finite displacements is carried out on a 12 bladed-disk finite element model. The paper is based on a computational methodology previously developed by the authors. It insists on the necessity to carefully optimize all the involved numerical parameters to get the nonlinear mistuned response of each considered detuned configuration with an optimal balance between response accuracy and computational costs. We then have to be very careful with the construction of an adapted scalar quantity of interest for defining the detuning optimization problem. Direct computations allowing for all possible detuned configurations to be considered allow for obtaining a full data basis. A meticulous post-processing shows the existence of a few detuned configurations, that inhibits the mistuning amplification effects of the pure mistuned bladed-disk.

NOMENCLATURE

nb_1 number of blades of type 1
nb_2 number of blades of type 2
$\underline{a}^{\ell}_M$ deterministic observation characterizing the most important values taken by $A^{\ell}(\theta_k) = a^{\ell,k}$
ℓ numbering of a given detuned configuration.
n_c number of all the possible configurations.
n_{sim} number of Monte Carlo realizations.
n_w number of blades.
$q^{c,\ell}$ amplification factor computed with HFCM from $\mathbf{w}^{c,\ell}$.
$w_j^{c,\ell}$ $= 0$ if j of type 1, $= 1$ if j of type 2.
$\mathbf{w}^{c,\ell}$ vector defining detuned configuration ℓ.
M order of the reduced-order model.
N order of the cyclic symmetry
Q order of the random matrices
$A^{\ell}(\theta_k) = a^{\ell,k}$ Realization θ_k of the maximal displacement norm over the blades and the frequency band of analysis related to detuned configuration ℓ
$J^{\ell}_{\max}(\theta_k) = j^{\ell,k}_{\max}$ Realization θ_k of the most responding blade over the frequency band of analysis and related to detuned configuration ℓ
$Y^{\ell}(j, 2\pi\nu_i, \theta_k)$ Realization θ_k of the displacement norm related to blade j, at frequency ν_i and related to detuned configuration ℓ
$Y^{\ell}_{\max}(2\pi\nu_i, \theta_k)$ Realization θ_k of the displacement norm over the blades, at frequency ν_i and related to detuned configuration ℓ
$\mathbf{X}^{\ell}(j, 2\pi\nu_i, \theta_k)$ Realization θ_k of the displacement vector of blade j, at frequency ν_i and related to detuned configuration ℓ
$\mathbb{B}$ frequency band of analysis
ν_i given frequency
θ_k given realization
HFCM High-Fidelity Computational Model.

*Address all correspondence to this author.

NL-SROM NonLinear Stochastic Reduced Order Model.

INTRODUCTION

The vibrational behavior of turbomachines is known to be particularly complex, requiring the construction of predictive computational models that have also to be efficient in terms of numerical costs. One of the issues concerns the mistuning caused by the small variations of the mechanical properties from one sector to another one, induced by the manufacturing tolerances or by the wear and tear of the structure. Such phenomenon can generate strong localization effects yielding subsequent dynamical amplifications of the forced response with respect to the perfect cyclic symmetry case [1–3]. This amplification strongly affects the fatigue life of the blades, which can cause safety problems and impair the proper operation of turbomachines. Many research have been carried out on this subject, requiring the use of probabilistic approaches for modeling the random character of the mistuning combined to the construction of reduced-order models [4–8] when linear assumption is considered. There also exist other phenomena that can strongly affect the vibrational behavior of the bladed disk and that have to be the subject of a dedicated modeling. The presence of nonlinearities increases the complexity of the forced response analysis because couplings and energy transfers can strongly modify the position and the nature of the resonances of the bladed disk. In particular, due to technological evolutions that involve lighter materials and thinner blades, the nonlinear geometrical effects induced by finite displacements cannot longer be neglected. The main difficulties concerning the modeling of these nonlinear geometrical effects concern the construction of adapted nonlinear reduced-order models that have to be efficient not only in terms of computational costs but also in terms of predictability. These aspects have also been investigated in the more general context of thin and slender structures [9–12]. Concerning the context of turbomachines, various research can be found for the deterministic case [13, 14], but also in presence of contact nonlinearities [15] or in presence of mistuning [16].

The intentional mistuning, also called detuning, consists in voluntarily breaking the cyclic symmetry of the structure by using partial or alternating patterns of different sector types. The detuning allows for spreading the frequencies of adjacent blades and thus for reducing the interaction between them. As a consequence, the drastic amplification and localization effects caused by the random mistuning can be greatly reduced. Such technology is particularly relevant because it is a way for reducing the response amplification levels that are induced by the unavoidable random mistuning while increasing its robustness. It has been thoroughly studied in the framework of linear dynamics [17–21].

In a context of sustainable development, technological innovations have to be compatible with energy and environmental issues. This gives rise to the development and to the use of lighter materials, that have to be capable of high thermo-mechanical resistance and of long durability, so that it may be possible that the blade displacements respond in its nonlinear vibration range. In this context, a computational methodology and a robust analysis of the geometrical nonlinear effects on several detuned configurations of mistuned bladed disk have been proposed in [22]. The results underline a complex nonlinear dynamical behavior and highlight a sensitivity of the nonlinear response to the detuning in presence of mistuning. Nevertheless, a too few number of detuned configurations is available and is not sufficient to perform a full optimization analysis with respect to the set of all possible detuned configurations of mistuned structures. Indeed, this latter one has a huge dimension that increases exponentially with respect to the number of blades.

The manuscript presents a numerical validation concerning the detuning optimization of a mistuned 12 bladed-disk structure in presence of geometrical nonlinearities. The theoretical background that concerns the formulation, the methodology, the computational model including the construction of the NL-SROM (NonLinear Stochastic Reduced-Order Model) and the use of the nonparametric probabilistic approach for the mistuning modeling [23, 24] and all the dedicated algorithms can be found in [16, 22, 25, 26].

In a first part, the computational analysis of a full data basis constituted of the set of all possible detuned configurations using a representative computational model of a 12-bladed-disk structure is carried out. The post-processing analysis then allows for constructing the exact solution of the detuning optimization problem.

COMPUTATIONAL METHODOLOGY TO GET A FULL DATA BASIS FOR THE MISTUNED STRUCTURE IN A NONLINEAR DETUNING OPTIMIZATION CONTEXT

In this Section, the computational model of the tuned structure is described in details. Note that the detuning optimization of the mistuned structure in presence of geometrical nonlinearities is then performed from such deterministic computational model. The numerical parameters are adjusted through convergence analyses related to the undetuned/mistuned blisk in order to optimize for the best the computational costs.

Nonlinear boundary value problem of a detuned system

In this paragraph, the nonlinear boundary value problem concerning any given detuned configuration is quickly described. The upperscript ℓ that will be used for describing a given detuned configuration is removed for a better readability.

Let Ω be the three-dimensional bounded domain of the physical space $\mathbb{R}^3$ corresponding to the steady configuration of a de-

tuned structure observed in the rotating frame that is defined as the reference configuration of the boundary value problem [27]. The boundary $\partial\Omega$ is such that $\partial\Omega = \Gamma_0 \cup \Gamma_{\mathbf{E}}$ with $\Gamma_0 \cap \Gamma_{\mathbf{E}} = \emptyset$ and the external unit normal to boundary $\partial\Omega$ is denoted by $\mathbf{n} = (n_1, n_2, n_3)$. The boundary part Γ_0 corresponds to the fixed part (in the rotating frame) of the structure whereas the boundary part $\Gamma_{\mathbf{E}}$ is submitted to an external surface force field. A total Lagrangian formulation is chosen. Consequently, the mechanical equations are written with respect to the reference configuration in the rotating frame. Let $\mathbf{x} = (x_1, x_2, x_3)$ be the position of a point belonging to domain Ω. The displacement field expressed with respect to the reference configuration is denoted as $\mathbb{x}(\mathbf{x},t) = \big(\mathbb{x}_1(\mathbf{x},t), \mathbb{x}_2(\mathbf{x},t), \mathbb{x}_3(\mathbf{x},t)\big)$. It should be noted that the surface force field $\mathbf{G}(\mathbf{x},t)) = \big(G_1(\mathbf{x},t)), G_2(\mathbf{x},t)), G_3(\mathbf{x},t)\big)$ acting on boundary $\Gamma_{\mathbf{E}}$ and the body force field $\mathbf{g}(\mathbf{x},t)) = \big(g_1(\mathbf{x},t)), g_2(\mathbf{x},t)), g_3(\mathbf{x},t)\big)$ acting on domain Ω correspond to the Lagrangian transport into the reference configuration of the physical surface force field and to the physical body force field applied on the deformed configuration.

The nonlinear boundary value problem is written, for $i = 1,2,3$ and using the classical convention for summations over repeated indices, as

$$\rho \frac{\partial^2 \mathbb{x}_i}{\partial t^2} + 2\rho\, r_{ik} \frac{\partial \mathbb{x}_k}{\partial t} + \rho\, r_{ik}\, r_{k\ell}(x_\ell + \mathbb{x}_\ell) = \tag{1}$$

$$\frac{\partial \left(F_{ij} S_{jk}\right)}{\partial x_k} + g_i(t) \quad \text{in} \quad \Omega \tag{2}$$

$$\mathbb{x}_i = 0 \quad \text{on} \quad \Gamma_0\,, \tag{3}$$

$$F_{ij} S_{jk} n_k = G_i(t) \quad \text{on} \quad \Gamma_{\mathbf{E}}\,, \tag{4}$$

in which $\rho > 0$ is the mass density expressed in the reference configuration, where the (3×3) matrix $[\mathbf{r}(\Omega)]$ whose component $[\mathbf{r}(\Omega)]_{ij}$ is denoted as r_{ij} for the sake of clarity, is such that $[\mathbf{r}(\Omega)]_{ij} = r_{ij} = -\Omega\,\varepsilon_{ij3}$, where ε_{ijk} is the Levi-Civita symbol such that $\varepsilon_{ijk} = \pm 1$ for an even or odd permutation and $\varepsilon_{ijk} = 0$ otherwise. In Eq. (4), $\{F_{ij}\}_{ij}$ is the deformation gradient tensor whose components F_{ij} are defined by $F_{ij} = \mathbb{x}_{i,j} + \delta_{ij}$, in which δ_{ij} is the Kronecker symbol such that $\delta_{ij} = 1$ if $i = j$ and $\delta_{ij} = 0$ otherwise and where $\mathbb{x}_{i,j}$ denotes the partial derivative $\partial \mathbb{x}_i / \partial x_j$. For a linear elastic material, the second Piola-Kirchoff symmetric stress tensor $\{S_{ij}\}_{ij}$ is written as $S_{ij} = \sigma^{(g)}_{ij} + a_{ijk\ell} E_{k\ell}$, in which $\{\sigma^{(g)}_{ij}\}_{ij}$ is the symmetric Cauchy stress tensor acting on the reference configuration observed in the rotating frame. The fourth-order elasticity tensor $\{a_{ijk\ell}\}_{ijk\ell}$ satisfies the usual symmetry and positive-definiteness properties. The Green strain tensor $\{E_{ij}\}_{ij}$ is written as the sum of linear and nonlinear terms such that $E_{ij} = \varepsilon_{ij} + \eta_{ij}$, in which $\varepsilon_{ij} = (\mathbb{x}_{i,j} + \mathbb{x}_{j,i})/2$ and where $\eta_{ij} = \mathbb{x}_{s,i}\mathbb{x}_{s,j}/2$.

Description of the finite element model

In this paragraph, the finite element model of the tuned structure of the blisk is described.

The structure under consideration is a blisk with order $N = 12$ and with $n_w = N = 12$ blades whose finite element computational model is constructed with hexahedral solid finite elements with 8 nodes. The finite element mesh is issued from [28] for which the order of the cyclic symmetry has been modified from 24 to 12 as also used in [21]. The main motivation of such reduction of the number of blades is to decrease the number of possible detuning patterns in order to have a reasonable number of detuning possibilities, as previously explained. In the present case, the aim is to constitute a full reference data basis in the nonlinear mistuned/detuned context. Indeed, when the detuning concept is approached with 2 possible types of blades, there are 352 possible detuned configurations when $N = 12$ that reduces the number of possibilities by a factor of almost $2^{N-1} \simeq 2\,000$ with respect to a structure with cyclic symmetry of order $2N = 24$. Let $(0, \mathbf{X}, \mathbf{Y}, \mathbf{Z})$ be the Cartesian reference coordinate system for which $(0, \mathbf{Z})$ coincides with the rotational axis for the blisk. Fig. 1 shows the finite element mesh of the blisk whose computational characteristics are summarized in Table 1. There are $n = 27\,108$ degrees of freedom (dof). The blisk is made up of a homogeneous and isotropic material with mass density $7\,860\,Kg/m^3$, Poisson ratio 0.25, and Young modulus $2\times 10^{11} N/m^2$. A Dirichlet condition is applied along the interfaces toward adjacent stages [28]. The fundamental frequency of the blisk is $\nu_0 = 977.32\,Hz$. A Rayleigh damping model is added for the blisk, with parameters $\mathbb{\alpha} = 78.67\,s^{-1}$ and $\mathbb{\beta} = 3.69\times 10^{-7}\,s$ chosen such that the critical damping rate $\xi(2\pi\nu)$ belongs to $[0.0054, 0.008]$ for $\nu \in [900\,, 6\,000]\,Hz$.

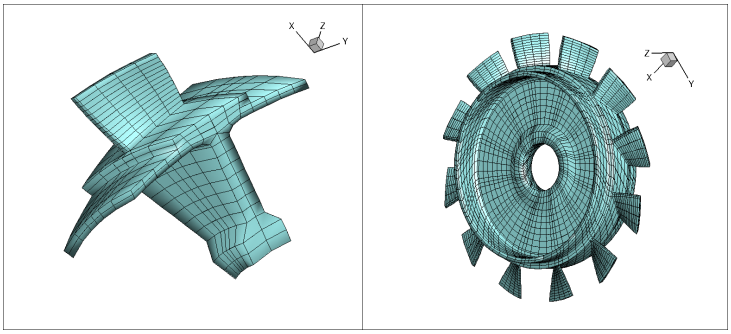

FIGURE 1. Finite element mesh of the blisk: blade sector (left figure), full blisk (right figure)

Modal characteristics of the tuned blisk

The eigenfrequencies (natural frequencies) of the structure are computed using the cyclic symmetry. Fig. 2 displays the

	Elements	Nodes	dof
Sector	476	846	2151
Full model	5712	9036	27108

TABLE 1. Computational characteristics of the finite element model

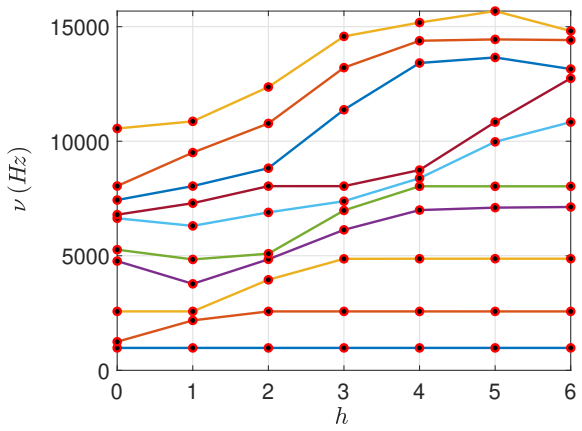

FIGURE 2. Graph of the eigenfrequencies ν of the tuned blisk with respect to its circumferential wave number h

eigenfrequencies of the tuned blisk with respect to its circumferential wave number. The graph exhibits several veerings. Let $\nu_{h,i}$ be the eigenfrequency number i related to the number h of nodal diameters. In the present case, the veering corresponding to $h=2$ nodal diameters corresponds to (double) eigenfrequency $\nu_{2,4}=4\,845.18\,Hz$ that is related to a dominant blade motion and to (double) eigenfrequency $\nu_{2,5}=5\,091.09\,Hz$ that is related to a blisk global motion.

Choice of the external excitation and time-frequency sampling

Since we are interested in the forced response of the structure, the presence of geometrical nonlinearities requires to solve the nonlinear dynamical equations in the time domain. The time-dependent external excitation is modeled by the $\mathbb{R}^n$-vector $\mathbf{F}(t)$ whose block decomposition according to each sector is given by $\mathbf{F}(t)=\left(\mathbf{F}^0(t),\ldots,\mathbf{F}^{N-1}(t)\right)$ such that

$$\mathbf{F}^j(t)=s_0\,g^j(t)\,\mathbb{F}\quad,\quad j\in\{0,1,\ldots,N-1\}\,,$$

in which s_0 is the load intensity that allows the nonlinearity rate to be calibrated, $t\mapsto g^j(t)$ is a square integrable real-valued function on $\mathbb{R}$, which characterizes the time evolution of the load, and where $\mathbb{F}$ is a $\mathbb{R}^{\overline{n}}$-vector describing the space localization of the load related to a given sector, in which integer $\overline{n}$ is equal to n/N. Time function g^j differs from one sector to another one by a constant phase shift $\varphi_j=(4\pi j)/N$. This choice of the phase allows the modes with $h=2$ nodal diameters to be excited for the linearized dynamical system. Function $g^j(t)$ is then defined so that its Fourier transform $\nu\mapsto g^j(2\pi\nu)$ is such that $|g^j(2\pi\nu)|=1$ if ν belongs to $\mathbb{B}_e=[\nu_{\min};\nu_{\max}]$, with $\nu_{\min}=4\,700\,Hz$, $\nu_{\max}=5\,200\,Hz$ and which allows for uniformly exciting the structure in band $\mathbb{B}_e$ [16,22]. From a numerical point of view, the computation is carried out on a truncated time domain $\mathbb{T}=[t_{\rm ini},t_{\rm ini}+T]$. The initial time is chosen as $t_{\rm ini}=-0.06\,s$ yielding a null initial load. The time duration $T=0.128\,s$ is then adjusted so that the system be returned at its equilibrium state within a given numerical tolerance for both linear and nonlinear computations.The sample frequency ν_e and the number of time steps are then chosen as $\nu_e=64\,000\,Hz$ and $n_t=8\,192$ yielding a constant sampling time step $\delta t=15.6\times10^{-6}\,s$ and a constant sampling frequency step $\delta\nu=7.8125\,Hz$. The spatial repartition of the external load described by the normalized vector $\mathbb{F}$ is such that an external point load is applied along all directions at the excitation nodes located at the tip of each blade with a constant phase shift $\pi/3$. The load intensity s_0 is adjusted to get sufficient geometrical nonlinear effects that modify the vibrational behavior of the blisk.

About the convergence analyses

Each detuned configuration of the blisk in presence of random mistuning is modeled by a nonlinear stochastic reduced-order model (NL-SROM) whose methodology of construction is not given in this paper. For a given detuned configuration, the NL-SROM is obtained from the finite discretization of the nonlinear equations (1-4), for which the physical displacements are projected on a vector basis [16, 22] that allows for obtaining a deterministic nonlinear reduced-order model [25]. The mistuning is assumed to only affect the linear elastic internal force and the nonlinear forces, which are therefore uncertain. Note that the nonlinear internal forces are directly evaluated in the reduced space, by direct numerical evaluation from the finite element model [25]. Uncertainties are implemented from the deterministic nonlinear reduced-order model using the nonparametric probabilistic approach [23, 24, 26]. As a consequence, there are several numerical parameters that are involved in the construction of the nonlinear mistuned forced response of the blisk.

It is essential to underline that a series of convergence analyses has to be carefully performed with respect to all the numerical parameters that are involved in the construction of the nonlinear mistuned response of the blisk. These convergence analyses have been made for the tuned configuration of the blisk, in presence of mistuning and are briefly summarized. The frequency band of analysis $\mathbb{B}$ is chosen as $\mathbb{B}=[300\,,6\,000]\,Hz$. A sensitivity analysis with respect to the load intensity s_0 yields $s_0=10\,N$ that corresponds to a situation for which nonlinear effects occurs,

meaning that the structure responds outside the frequency band of excitation $\mathbb{B}_e$. The efficiency and the accuracy of the Newmark time integration scheme coupled with a Newton-Raphson procedure is investigated with respect to time step δt. If the convergence is relatively quick when analyzing the structure in the excitation frequency band, it is shown that a stability is obtained on the whole frequency band of analysis $\mathbb{B}$ for time steps lower than $\delta t = 15.6\times10^{-6}\,s$. A convergence analysis is also set with respect to the order M of the NL-SROM, to the order Q of the random matrices corresponding to an uncertainty level $\delta_K = 0.1$ and to the number $n_{\rm sim}$ of realizations yielding a good approximation for $M = 72$, $Q = 440$ and $n_{\rm sim} = 400$. All these numerical computations are essential (1) to better understand the dynamic behavior of the blisk and (2) to optimize for the best the computational costs while keeping a predictive computational model that ensures a good accuracy on the nonlinear dynamical response. It is essential to underline that all these convergence analyses have to be carried out meticulously. Indeed the aim of this work concerns the optimization of the detuning of the blisk in presence of mistuning.

COMPUTATIONAL RESULTS CONCERNING THE NONLINEAR DETUNING OPTIMIZATION OF THE MISTUNED STRUCTURE

In this Section, after defining the modeling of the detuning, the observation of interest denoted by $q^{c,\ell}$ is obtained from a direct optimized computational approach as a function of a detuned configuration denoted by $w^{c,\ell}$. Note that quantity $q^{c,\ell}$ represents the amplification factor of a detuned structure (represented by upperscript ℓ) with respect to its tuned counterpart. It should also be noted that a careful optimization of the computational model of the tuned structure called HFCM (High Fidelity Computational Model) have been previously carried out with respect to all the parameters controlling the numerical algorithms .

The detuning optimization is carried out as a post-processing analysis of the full data basis. In the present numerical study, all the computations are distributed according to the number $n_{\rm sim}$ of Monte Carlo realizations and are made on workstations with 1536 GB RAM and 30 cores (Intel(R) Xeon(R) Platinum 8168 CPU@2.9Ghz). The generated elapsed time is about 6 hours to perform 1 computation corresponding to the nonlinear analysis of 1 detuned pattern in presence of mistuning, which means that the construction of the full data basis requires an elapsed time of about 88 days of computations.

About the modeling of the detuning

The computational model of the detuned blisk is constructed from the knowledge of two identical meshes of two different sector types denoted as 1 and 2. The reference sector 2 is obtained from sector 1 by decreasing the Young modulus of the blade from $\text{Young}_1 = 2.00\times10^{11}\,\text{N/m}^2$ to $\text{Young}_2 = 1.80\times10^{11}\,\text{N/m}^2$. Let us denote by nb_1 and nb_2 the number of blades of type 1 and type 2 in a detuned configuration. Let $n_c(\text{nb}_1,\text{nb}_2)$ be the number of possible detuned configurations having nb_1 and nb_2 blades of type 1 and 2 respectively. Let n_c be the total number of detuned configurations for all the possible values of nb_1 and nb_2. For the tuned blisk with cyclic symmetry of order $N = 12$, Table 2 gives the number $n_c(\text{nb}_1,\text{nb}_2)$ of detuned configurations as a function of the number nb_1 and nb_2 of blades of type 1 and 2. There are a total number of $n_c = 352$ possible detuned configurations. As shown in [21], the number of possible configurations exponentially increases with the number of blades N and is close to $\dfrac{2^N}{N}$ when considering 2 different blades. Since it is wished to obtain a full data basis that explores the set of all possible detuned configurations in order to ensure the existence and an order of magnitude of possible improving detuned configurations (that inhibates the amplifications induced by the pure mistuning situation), the investigation of the detuning is limited to 2 distincts blades using a cyclic symmetry of order $N = 12$.

nb_1	12	11	10	9	8	7	6	5	4	3	2	1	0
nb_2	0	1	2	3	4	5	6	7	8	9	10	11	12
n_c	1	1	6	19	43	66	80	66	43	19	6	1	1

TABLE 2. Number $n_c(\text{nb}_1,\text{nb}_2)$ of detuned configurations as a function of the number nb_1 and nb_2 of blades of type 1 and 2.

The objective is to find the optimal configuration that will reduce for the best the response amplification induced by mistuning. Another objective is to have a complete knowledge of the nonlinear dynamical behavior of all possible detuned configurations in order to constitute a reference data basis.

Choice of the observation

The pure mistuning case corresponds to the usual situation for which the blisk is described with a tuned configuration in presence of mistuning. In that particular case, the deterministic case corresponds to a structure with a perfect cyclic symmetry with order N. The usual mistuning analyses, whether it is in a linear or nonlinear context, characterize the mistuning effects by introducing a random amplification factor that is expressed with respect to the deterministic resonance of the structure with perfect cyclic symmetry.

The detuned configuration in presence of mistuning is defined by a given distribution of the blades of type 1 and 2. The detuned configuration number ℓ is then represented by a vector $\mathbf{w}^{c,\ell} \in \{0,1\}^{n_w}$ whose component $w_j^{c,\ell}$ is equal to 0 or 1 whether the blade is of type 1 or of type 2. Let us recall that for a given mistuning level, the drastic mistuning effects yield a response

amplification with respect to its deterministic counterpart. The objective is to find detuned configurations whose mistuning effects induce less amplification than the one obtained with the tuned configuration in presence of mistuning. The idea is then to define a scalar quantity that is able to quantify the mistuning effects of the detuned configuration with respect to the unavoidable mistuning effects of the tuned configuration.

Let $\mathbf{X}^\ell(j,2\pi\nu_i,\theta_k)$ be the $\mathbb{C}^{3n_b}$-vector of the realization θ_k of the $3n_b$-displacement dofs of blade number $j\in\{1,\ldots,n_w\}$ in the frequency domain, taken at frequency ν_i, and corresponding to the detuned configuration number ℓ. Note that this random observation is obtained from the NL-SROM related to detuned configuration ℓ.

For blade number j of configuration ℓ, at frequency ν_i, and for realization θ_k, we define the scalar observation $Y^\ell(j,2\pi\nu_i,\theta_k)=\|\mathbf{X}^\ell(j,2\pi\nu_i,\theta_k)\|$. Since the mistuning context requires to consider the resonance of the most responding blade, we define the $\mathbb{R}^+$-valued random variable A^ℓ whose realization $a^{\ell,k}=A^\ell(\theta_k)$ is such that

$$a^{\ell,k}=\max_j\{\max_i Y^\ell(j,2\pi\nu_i,\theta_k)\}\,. \tag{5}$$

We define the associated random variable $J^\ell_{\max}$ whose realization $j^{\ell,k}_{\max}=J^\ell_{\max}(\theta_k)$ is such that

$$j^{\ell,k}_{\max}=\arg\max_j\{\max_i Y^\ell(j,2\pi\nu_i,\theta_k)\}\,. \tag{6}$$

In order to get a robust scalar quantity for characterizing the random nonlinear dynamical behavior of the blisk, an estimate of the maximum extreme value statistics of random variable A^ℓ is introduced. It should be noted that, for a fixed ℓ-configuration, the maximum is used so that all realizations are in the confidence domain with the greatest probability. This estimation is constructed as follows. The available number of Monte Carlo numerical simulations is written as $n_{\rm sim}=\nu_r\,\nu_e$ (for $n_{\rm sim}=500$, $\nu_e=10$ and $\nu_r=50$). We then define for $r\in\{1,\ldots,\nu_r\}$ quantity $\underline{a}^\ell_M$, such that

$$\underline{a}^\ell_M=\frac{1}{\nu_r}\sum_{r=1}^{\nu_r}a^{\ell,r}_M \text{ with } a^{\ell,r}_M=\max_{k\in\{\nu_e(r-1)+1,\ldots,r\nu_e\}}a^{\ell,k}\,. \tag{7}$$

It should be noted that such quantity of interest is neither issued from a mean value or from an extreme value but is defined as an average of a set of $\nu_r=50$ maxima taken in a subset of $\nu_e=10$ realizations. This allows for capturing information on the maxima with a reasonable number of available Monte Carlo numerical simulations. The observation of the detuned ℓ-configuration with mistuning is then defined as the amplification factor $q^{c,\ell}$ with respect to its tuned counterpart with pure mistuning, that is written as

$$q^{c,\ell}=\frac{\underline{a}^\ell_M}{\underline{a}^{\rm t}_M}\,, \tag{8}$$

in which superscript t is related to the tuned configuration.

It should also be noted that the chosen external load corresponds to a narrow-frequency band of excitation so that the linearized detuning optimization problem has no real interest. Indeed it cannot be properly achieved since the natural frequencies of most detuned configurations do not belong to this narrow excitation frequency range and since the structure only can respond in the excitation frequency band.

Detuned configurations that decrease the amplification of the nonlinear response induced by the mistuning

A detuned configuration ℓ, which yields a nonlinear mistuned response level that is smaller than the one obtained with the tuned configuration in presence of mistuning, is characterized by $q^{c,\ell}<1$. Such configuration belongs to the set of optimal detuned configurations. In the detuning process, the tuned configuration $\mathbf{w}^{c,{\rm t}}=[000000000000]$ in presence of mistuning is considered and yields amplification $q^{c,{\rm t}}=1.0000$. The detuning is defined around this tuned configuration. This subset corresponds to $n_c=216$ possible detuned configurations for which the number nb_2 of blades of type 2 is less than or equal to $n_w/2=6$ (see Table 2). From now on, only detuned configurations corresponding to $n_c=216$ possible detuned configurations will be considered. This assumption is motivated by the fact that (1) the worst detuned configuration belongs to this subset, (2) there is only one improving detuned configuration that has a number nb_2 of blades with type 2 greater than 6 amongst the 14 improving detuned configurations and (3) that most of the detuned configurations having a majority of blades with type 2, have a subsequent amplification factor. Fig. 3 shows the graph of $j\mapsto q^{c,\ell_j}$ where q^{c,ℓ_j} are sorted by increasing order for $n_c=216$. It can be shown that the amplification factor increases from $q^{c,\ell_1}=q^{c,104}=0.9476$ until $q^{c,\ell_{352}}=q^{c,9}=1.1774$ corresponding to detuned configurations defined by $\mathbf{w}^{c,104}=[000100100101]$ and $\mathbf{w}^{c,9}=[010001110011]$. The tuned configuration $w^{c,t}$ corresponds to $\ell=49$. Figure 4 summarizes the results obtained with these improving detuned configurations. Note that there is only one configuration that presents a subcyclicity with order $s=2$ with $q^{c,\ell}=0.9995$. The other improving detuned configurations have no particular cyclicity.

A careful attention is also paid to the 10 detuned configurations that present a cyclic symmetry $s\in\{2,3,4,6\}<N$. The

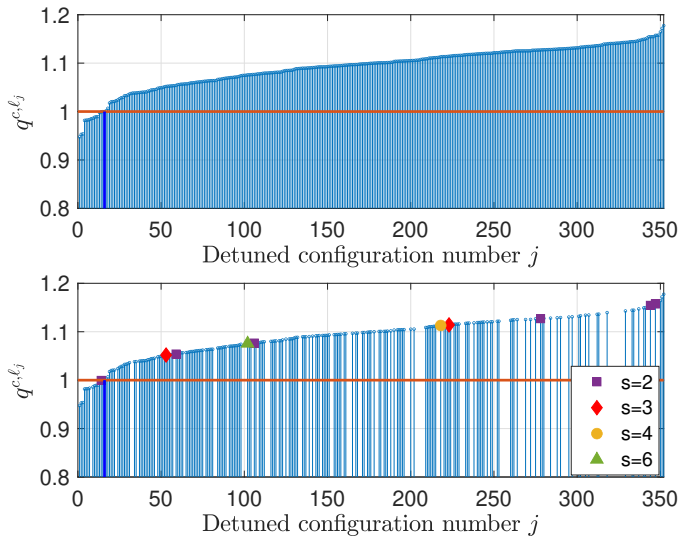

FIGURE 3. Dynamical amplification factor according to detuned configuration. Graph of function $j \mapsto q^{c,\ell_j}$ for the $n_c = 352$ possible detuned configurations (upper graph) and for the $n_c = 216$ detuned configurations with a number of blades with type 2 less than or equal to 6 (lower graph). Subcyclicity order s is given for $s = 2$ (purple square symbol), $s = 3$ (red diamond symbol), $s = 4$ (orange bullet symbol) and $s = 6$ (green triangle symbol).

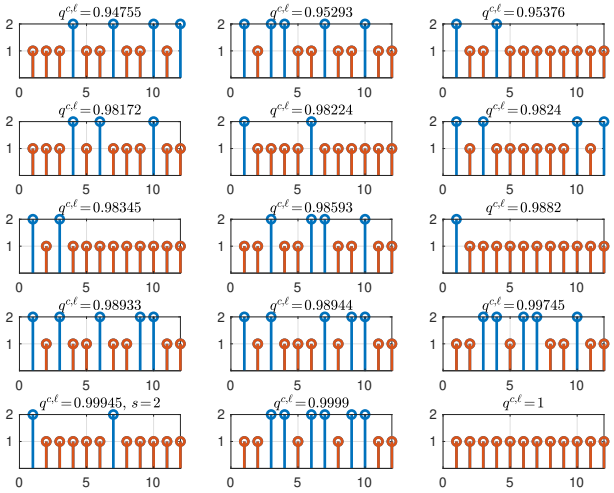

FIGURE 4. Characteristics of the improving detuned configurations.

characteristics are summarized in Figure 5 and the corresponding amplification factors are represented by symbols in Fig. 3. As shown in Fig. 4, except for detuned configuration with $s = 2$ and with an amplification factor $q^{c,211} = 0.9995 \simeq 1$ that slightly inhibits the mistuning effects, these subcyclic configurations give rise to an amplification between 5% and 16% with respect to the

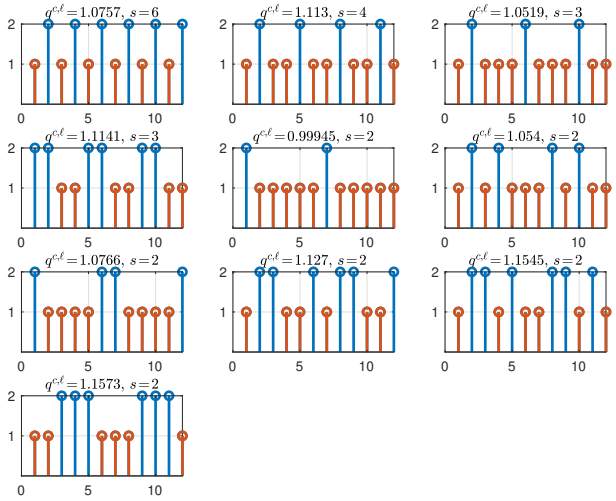

FIGURE 5. Characteristics of the detuned configurations with a subcyclicity s

pure mistuning situation.

Nonlinear analysis of the mistuned response of the best and the worst detuned configurations

The results are analyzed for the following detuned configurations: the tuned configuration corresponding to the pure mistuning case ($\ell = 49$), the best detuned configuration ($\ell = 104$), and the worst detuned configuration ($\ell = 9$). Fig. 6 displays the graphs of $k \mapsto a^{\ell,k} = A^{\ell}(\theta_k)$ for $k = 1, \ldots, n_{\text{sim}}$, which describes the maximum displacement response over the frequency and the blades for each mistuning realization θ_k of the detuned configurations $\ell \in \{49, 104, 9\}$. By comparing these graphs, it can be seen that the best detuned configuration is characterized by slightly lower response levels but also by less scattered realizations with respect to the pure mistuned case (left figure). The realizations of the worst detuned configurations (right graph) are clearly more scattered with higher response levels. The distribution of the blades related to these detuned configurations are displayed in Fig. 7.

For a given detuned configuration ℓ and a fixed frequency ν, we introduce the real-valued random variable $Y^{\ell}_{\max}(2\pi\nu)$ whose realization θ_k is defined by

$$Y^{\ell}_{\max}(2\pi\nu, \theta_k) = Y^{\ell}(j^{\ell,k}_{\max}, 2\pi\nu, \theta_k)\,. \tag{9}$$

For detuned configurations $\ell \in \{49, 104, 9\}$, Figs. 8 to 10 display the graphs of the confidence region of the real-valued random function $\nu \mapsto Y^{\ell}_{\max}(2\pi\nu)$ for a probability level of 0.98.

The analysis of the graphs of the confidence region of the real-valued random function $\nu \mapsto Y^{\ell}_{\max}(2\pi\nu)$ for a probability level of 0.98 shows that the structural displacements are mainly located in the frequency band of excitation $\mathbb{B}_e$ but that there are

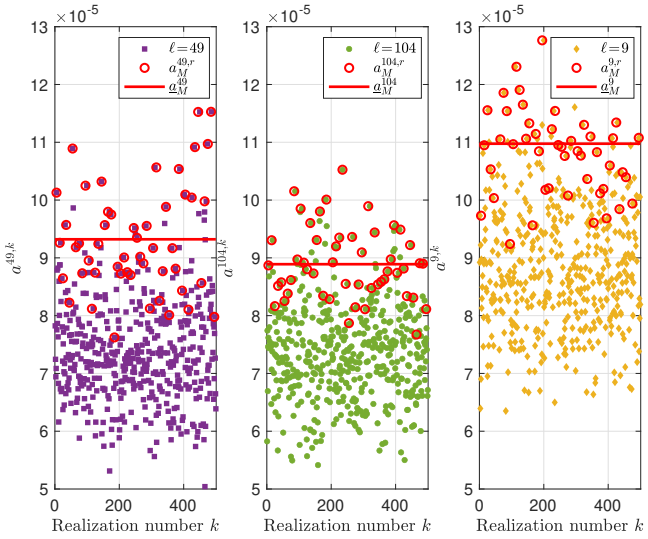

FIGURE 6. Analysis of the mistuned response for given detuned configurations: graph of realizations $k \mapsto a^{\ell,k} = A^{\ell}(\theta_k)$ (colored symbols), of realizations $(5r+10) \mapsto a_M^{r,\ell}$ (red circle) and value of constant $\underline{a}_M^{\ell}$ (red thick line) for the tuned configuration (pure mistuning) $\ell = 49$ (left figure), the best detuned configuration $\ell = 104$ (middle figure), and the worst detuned configuration $\ell = 9$ (right figure).

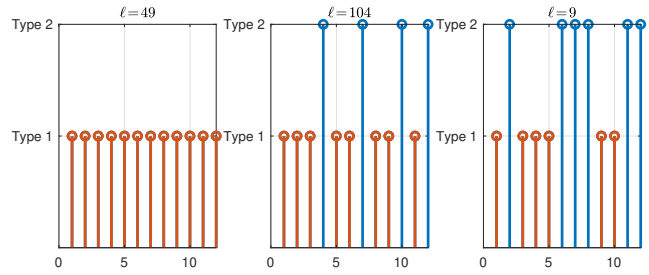

FIGURE 7. Analysis of the blade distribution corresponding to the pure mistuned configuration (left graph), the best detuned configuration (middle graph), and the worst detuning case (right graph).

also new resonances occurring below the frequency band of excitation $\mathbb{B}_e$ that are induced by the geometrical nonlinearities. The amplitudes of these new resonances correspond to the indirect excitation of the first blade modes of the blisk and are of a lower order of magnitude in the present case, probably because the blades are not very slender. Fig. 11 shows a zoom of these confidence regions around the excitation frequency band $\mathbb{B}_e$. It is clearly seen that the pure mistuned blisk have slightly more robust resonances that the one obtained with the detuned configurations in presence of mistuning. But the real interest is to verify that the optimal detuned configuration (middle graph) guarantees that the upper envelope of the confidence region stays below the critical level of response of the pure mistuned response. It is thus observed that the optimal detuned configuration yields a reduction of the maximum amplitude of about 12% with respect to the initial situation that corresponds to the pure mistuning case. Another observation is that the worst detuned configuration yields an amplification of about 11% with respect to the initial situation that corresponds to the pure mistuning case. Furthermore, let $z_{\max}^{\ell,+}(2\pi\nu)$ be the upper bound of confidence region $Y_{\max}^{\ell}(2\pi\nu)$ normalized with respect to its pure mistuned counterpart. Figure 12 shows the graphs of $\nu \mapsto z_{\max}^{\ell,+}(2\pi\nu)$ for the 15 best and for the 15 worst detuning configurations. It can be seen that the first resonance that is also the main resonance of the pure mistuned system is the one that is involved in the detuning optimization process, the two other ones being robust to detuning optimization. To the contrary, the worst detuned configurations violate the critical level through the two first resonances. All these observations allow for assessing the efficiency of the optimization through the output of interest $q^{c,\ell}$.

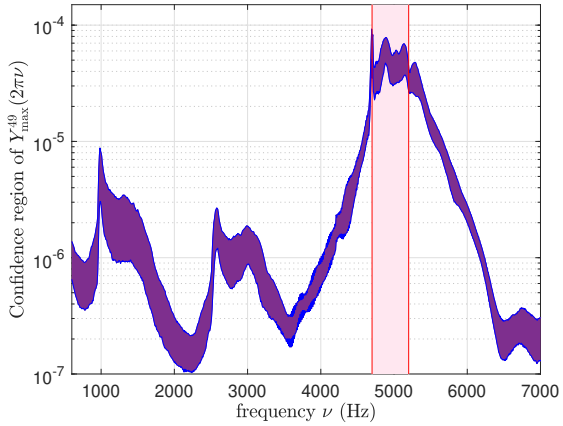

FIGURE 8. Analysis of the mistuned response for the tuned configuration: graph of the confidence region of $\nu \mapsto Y_{\max}^{\ell}(2\pi\nu)$ for a probability level of 0.98, corresponding to the pure mistuned configuration $\ell = 49$ (purple area). Excitation frequency band $\mathbb{B}_e$ is represented by the light pink area.

CONCLUSION AND DISCUSSION

We have presented an approach for the optimization of the detuning in presence of random mistuning and geometrical nonlinearities for bladed disks, based on the use of high-fidelity computational models. This very challenging problem has given rise to very little published work and remains an open subject. The difficulties we have addressed are related to the developments of

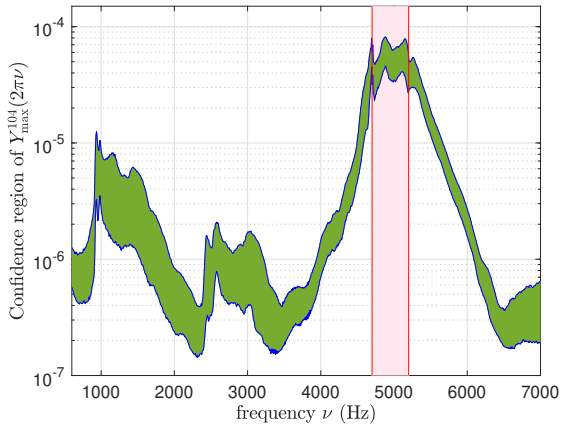

FIGURE 9. Analysis of the mistuned response for given detuned configurations: graph of the confidence region of $\nu \mapsto Y_{\max}^{\ell}(2\pi\nu)$ for a probability level of 0.98, corresponding to the best detuned configuration $\ell = 104$ (green area). Excitation frequency band $\mathbb{B}_e$ is represented by the light pink area.

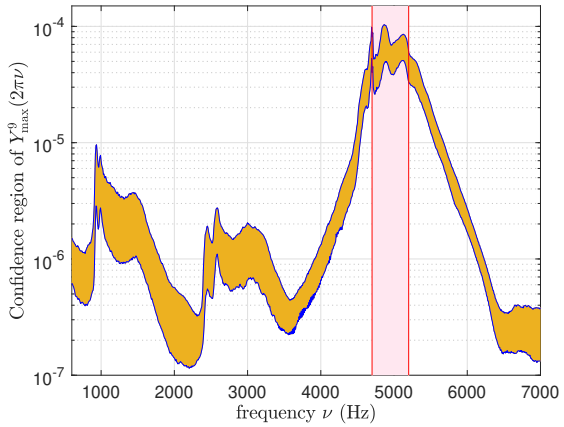

FIGURE 10. Analysis of the mistuned response for given detuned configurations: graph of the confidence region of $\nu \mapsto Y_{\max}^{\ell}(2\pi\nu)$ for a probability level of 0.98, corresponding to the worst detuned configuration $\ell = 9$ (orange area). Excitation frequency band $\mathbb{B}_e$ is represented by the light pink area.

an efficient computational methodology for reducing the computational cost, to the physics understanding of such stochastic nonlinear dynamical systems, and to the probabilistic formulation of the detuning optimization problem. Several results can be put forward.

A careful convergence analysis with respect to all numerical parameters must be performed to obtain a predictive solution with an optimal computational cost. This is essential for exploring a relatively large number of detuned configurations in the

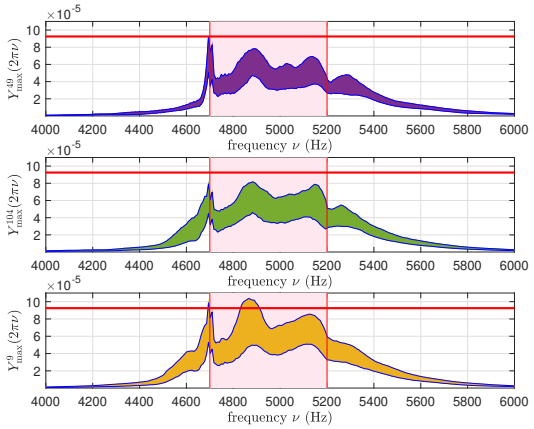

FIGURE 11. Analysis of the mistuned response for given detuned configurations: for a probability level of 0.98, zoom of the confidence region of $\nu \mapsto Y_{\max}^{\ell}(2\pi\nu)$ for the pure mistuned configuration $\ell = 49$ (upper graph), for the best detuned configuration $\ell = 104$ (middle graph), and for the worst detuned configuration $\ell = 9$ (lower graph). Critical level defined by the maximum of the upper envelope corresponding to the pure mistuned situation (red line).

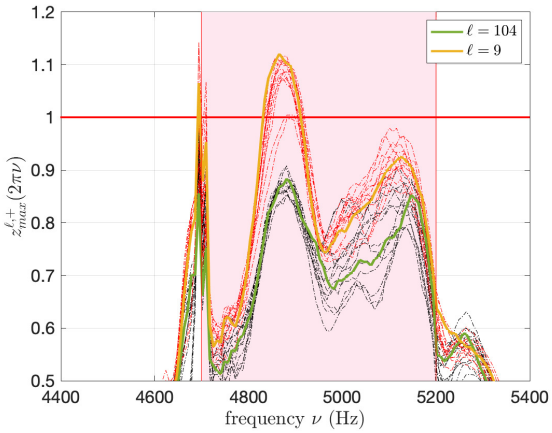

FIGURE 12. Analysis of the mistuned response for given detuned configurations: zoom of the upper bound of confidence region $\nu \mapsto z_{\max}^{\ell,+}(2\pi\nu)$ for the best detuned configuration $\ell = 104$ (green line), for the worst detuned configuration $\ell = 9$ (orange line), for the 15 best configurations (black dashed-dotted lines) and for the 15 worst configurations (red dashed-dotted lines). Critical level corresponding to the pure mistuned situation is set to 1 (red line).

context of the stochastic nonlinear mistuning analysis. It should be noted that the sensitivity analysis with respect to the time step used in the numerical resolution of the nonlinear coupled differential equations is particularly delicate, yielding a fast convergence in the excitation frequency band but a slow convergence in

the low-frequency range that is not directly excited by the external loading.

Another point of attention concerns the choice of the quantities of interest used in the formulation of the detuning optimization problem from a scalar-valued highly nonlinear cost function. It is found that there is a few number of optimal solutions with respect to the number of possible detuned configurations. It is also proved that the optimization problem is well-posed, yielding to robust optimal detuned configurations that are identified after post-processing analysis as detuned configurations for which the mistuning amplification effects are inhibited with respect to the pure mistuning situation.

The detuning patterns yielding the best optimal detuned configurations and yielding the worst amplification response levels have no particularly structure in terms of number of blades of different types and of blade distribution, which deserve further investigations to understand the complex mechanisms induced by the detuning. As expected, the sub-cyclic detuned configurations that present a cyclic symmetry with a lower cyclic order are sensitive to the mistuning and are not part of the optimal solutions.

The chosen external load corresponds to a narrow-frequency band of excitation so that the linearized detuning optimization problem has no real interest. Indeed it cannot be properly achieved since the natural frequencies of most detuned configurations do not belong to this narrow excitation frequency range and since the structure only can respond in the excitation frequency band. This is to underline that the nonlinear detuned optimization problem is of different nature because of the complex vibratory behavior induced by the geometric nonlinearities that appear themselves as an excitation that spreads the nonlinear response on the whole frequency band of analysis.

The availability of this full detuning data basis can also be viewed as a way to validate further optimization methodologies, by investigating the detuning optimization problem as a combinatorial optimization problem based on a probabilistic learning approach [29]. Such research open area could be of interest when considering bladed disk structures with a large number of blades.

ACKNOWLEDGMENT

The authors thank Pr. Christophe Pierre from the Illinois University concerning the use of the bladed-disk finite element model.

REFERENCES

[1] Whitehead, D., 1966. "Effects of mistuning on the vibration of turbomachine blades induced by wakes". *Journal of Mechanical Engineering Science,* ***8***(1), pp. 15–21.

[2] Ewins, D., 1969. "The effects of detuning upon the forced vibrations of bladed disks". *Journal of Sound and Vibration,* ***9***(1), January, pp. 65–69.

[3] Wei, S., and Pierre, C., 1988. "Localization phenomena in mistuned assemblies for cyclic symmetry - part ii: forced vibrations". *ASME Journal of Vibration, Acoustics, Stress, and Reliability in Design,* ***110***(4), pp. 439–449.

[4] Bladh, R., Castanier, M., and Pierre, C., 2001. "Component-mode-based reduced order modeling techniques for mistuned bladed disks. part 1: theoretical models". *ASME Journal of Engineering for Gas Turbines and Power,* ***123***(1), January, pp. 89–99.

[5] Yang, M.-T., and Griffin, J., 2001. "A reduced-order model of mistuning using a subset of nominal modes". *ASME Journal of Engineering for Gas Turbines and Power,* ***123***(3), October, pp. 893–900.

[6] Capiez-Lernout, E., and Soize, C., 2004. "Nonparametric modeling of random uncertainties for dynamic response of mistuned bladed-disks.". *ASME Journal of Engineering for Gas Turbines and Power,* ***126***(3), pp. 610–618.

[7] Mbaye, M., Soize, C., and Ousty, J.-P., 2010. "A reduced-order model of detuned cyclic dynamical systems with geometric modifications using a basis of cyclic modes". *ASME Journal of Engineering for Gas Turbines and Power,* ***132***(11), pp. 112502–1–9.

[8] Schwerdt, L., Panning-von Scheidt, L., and Wallaschek, J., 2021. "A model reduction method for bladed disks with large geometric mistuning using a partially reduced intermediate system model". *ASME Journal of Engineering for Gas Turbines and Power,* ***143***(7).

[9] Muravyov, A. A., and Rizzi, S., 2003. "Determination of nonlinear stiffness with application to random vibration of geometrically nonlinear structures". *Computers & Structures,* ***81***(15), pp. 1513–1523.

[10] Mignolet, M. P., Przekop, A., Rizzi, S. A., and Spottswood, S. M., 2013. "A review of indirect/non-intrusive reduced order modeling of nonlinear geometric structures". *Journal of Sound and Vibration,* ***332***(10), pp. 2437–2460.

[11] Wang, X., Mignolet, M. P., and Soize, C., 2020. "Structural uncertainty modeling for nonlinear geometric response using nonintrusive reduced order models". *Probabilistic Engineering Mechanics,* ***60***, p. 103033.

[12] Wang, X. Q., Khanna, V., Kim, K., and Mignolet, M. P., 2021. "Nonlinear reduced-order modeling of flat cantilevered structures: Identification challenges and remedies". *Journal of Aerospace Engineering,* ***34***(6), p. 04021085.

[13] Vakakis, A., 1992. "Dynamics of a nonlinear periodic structure with cyclic symmetry". *Acta Mechanica,* ***95***(1-4), pp. 197–226.

[14] Martin, A., and Thouverez, F., 2018. "Dynamic analysis and reduction of a cyclic symmetric system subjected to geometric nonlinearities". *Journal of Engineering for Gas*

Turbines and Power, ***141***(4).

[15] Delhez, E., Nyssen, F., Golinval, J.-C., and Batailly, A., 2021. "Reduced order modeling of blades with geometric nonlinearities and contact interactions". *Journal of Sound and Vibration*.

[16] Capiez-Lernout, E., Soize, C., and Mbaye, M., 2015. "Mistuning analysis and uncertainty quantification of an industrial bladed disk with geometrical nonlinearity". *Journal of Sound and Vibration,* ***356***(10), pp. 124–143.

[17] Castanier, M., and Pierre, C., 1998. "Investigation of the combined effects of intentional and random mistuning on the forced response of bladed disks". In Proceedings 34th AIAA/ASME/SAE/ASEE Joint Propulsion Conference and Exhibit, Cleveland OH ,July, 13-15 1998.

[18] Castanier, M., and Pierre, C., 2002. "Using intentional mistuning in the design of turbomachinery rotors". *AIAA journal,* ***40***(10), pp. 2077–2086.

[19] Choi, B.-K., Lentz, J., Rivas-Guerra, A. J., and Mignolet, M. P., 2003. "Optimization of intentional mistuning patterns for the reduction of the forced response effects of unintentional mistuning: formulation and assessment". *ASME Journal of Engineering for Gas Turbines and Power,* ***125***(1), 12, pp. 131–140.

[20] Mbaye, M., Soize, C., Ousty, J.-P., and Capiez-Lernout, E., 2013. "Robust analysis of design in vibration of turbomachines". *ASME Journal of Turbomachinery,* ***135***(2), p. 021008.

[21] Han, Y., Murthy, R., Mignolet, M., and Lentz, J., 2014. "Optimization of intentional mistuning patterns for the mitigation of the effects of random mistuning". *ASME Journal of Engineering for Gas Turbines and Power,* ***136***(06), p. 062505.

[22] Picou, A., Capiez-Lernout, E., Soize, C., and Mbaye, M., 2020. "Robust dynamic analysis of detuned-mistuned rotating bladed disks with geometric nonlinearities". *Computational Mechanics,* ***65***(3), pp. 711–730.

[23] Soize, C., 2000. "A nonparametric model of random uncertainties for reduced matrix models in structural dynamics". *Probabilistic Engineering Mechanics,* ***15***(3), pp. 277–294.

[24] Mignolet, M.-P., and Soize, C., 2008. "Stochastic reduced order models for uncertain geometrically nonlinear dynamical systems". *Computer Methods in Applied Mechanics and Engineering,* ***197***(45-48), pp. 3951–3963.

[25] Capiez-Lernout, E., Soize, C., and Mignolet, M., 2012. "Computational stochastic statics of an uncertain curved structure with geometrical nonlinearity in three-dimensional elasticity". *Computational Mechanics,* ***49***(1), pp. 87–97.

[26] Capiez-Lernout, E., and Soize, C., 2017. "An improvement of the uncertainty quantification in computational structural dynamics with nonlinear geometrical effects". *International Journal for Uncertainty Quantification,* ***7***(1), pp. 83–98.

[27] Desceliers, C., and Soize, C., 2004. "Non-linear viscoelastodynamic equations of three-dimensional rotating structures in finite displacement and finite element discretization". *International Journal of Non-Linear Mechanics,* ***39***(3), pp. 343–368.

[28] Bladh, R., Castanier, M., and Pierre, C., 2001. "Component-mode-based reduced order modeling techniques for mistuned bladed disks. part 2: application". *ASME Journal of Engineering for Gas Turbines and Power,* ***123***(1), January, pp. 100–108.

[29] Soize, C., and Ghanem, R., 2020. "Physics-constrained non-gaussian probabilistic learning on manifolds". *International Journal for Numerical Methods in Engineering,* ***121***(1), pp. 110–145.